A comparison of silver nanoparticles made by green chemistry and femtosecond laser ablation and injected into a PVP/PVA/chitosan polymer blend

ahmed waly (ahmedwaves20@yahoo.com)
amr abdelghany
ahmed tarabia

Research Article

Keywords: Silver nanoparticles, Laser ablated, green synthesized, PVA, PVP, chitosan

Posted Date: June 6th, 2022

DOI: https://doi.org/10.21203/rs.3.rs-1645059/v1

Abstract

Pristine samples of a polymer blend of polyvinylpyrrolidone (PVP)/ polyvinyl alcohol (PVA)/ chitosan filled with different concentrations of silver nanoparticles (AgNPs) were prepared using the casting method. The samples were then examined using various physical and antibacterial characterization techniques. Characterization studies showed that the blend provides a uniform and controlled distribution of AgNPs inside the polymeric matrix without the addition of any more stabilizers. The mean particle size for green and laser-ablated AgNPs was found to be 50 nm according to transmission electron microscopy (TEM) studies. Fourier transforms infrared (FTIR) studies showed the presence of characteristic main peaks corresponding to the vibrational groups which characterize the prepared samples. The interactions between the AgNPs and the blend were marked by changes in the intensity of vibrational peaks and spectral positions. X-ray diffraction (XRD) confirmed the structural modification within the PVP/PVA/chitosan matrix because of AgNPs filling. The change in the absorbance has been studied with the help of measured ultraviolet-visible spectroscopy (UV-Vis.) and therefore the optical band gap was calculated. The filling of AgNPs in the blend shows a broad peak at 427 nm because of the phenomenon of surface plasmon resonance (SPR) and its intensity increases with increasing filler concentration. The blend and the Ag-nanocomposite showed good antibacterial activity and caused a significant decrease in microbial growth (Escherichia coli) in 24 hours.

1. Introduction

Silver nanoparticles (AgNPs) are among the most important materials used in research and industrial fields in the current century. One of the most important characteristics of nanometric silver particles is the improvement of many physical and biological properties significantly over the bulk silver, which we find in changing the optical, electrical, and also antibacterial properties. AgNPs can be used in a variety of applications, such as antibacterial agents [1], sensors [2], solar cells [3], and electronics [4].

Polymer composites are one of the most interesting near-term means for taking the advantage of the important features of AgNPs. Polyvinyl alcohol (PVA) is a remarkable polymer because of its chemical and physical properties and has therefore drawn researchers' attention over the years. PVA is a biocompatible, chemically stable compound and has a semi-crystalline nature resulting from the role of the OH groups and hydrogen bonding [5]. It can create a strong interchain and intrachain hydrogen bonding and can also interact with other polymers via chemical bonding or hydrogen bonding between groups. PVA has major applications such as biomedicine, food packaging, and water filtration [6]. It has high dielectric strength, a good charge storage capacity, and optical and electrical properties that depend on the filling [7]. Additionally, PVA is used as a capping agent to control the nano-particles shape and size and to impart stability to many synthesized nanoparticles such as AgNPs.

Polyvinylpyrrolidone (PVP) is also a water-soluble polymer, a pH-stable, non-toxic, biodegradable, and biocompatible polymer that helps encapsulate and deliver lipophilic and hydrophilic drugs [8]. PVP can serve as a nanoparticle dispersant, reducing agent, growth modifier, and surface stabilizer depending on

specific synthesis conditions and material system. It was considered to be a potential material with very good film formability for potential applications in the manufacture of plastics, adhesives, protectants, coatings, paints, detergents, printing inks, and cosmetics [9].

Chitosan is a chitin-based natural polymer and has excellent non-toxic, antimicrobial, biocompatible, and biodegradable properties [10]. Chitin is found in the cell walls of fungi, arthropod exoskeletons such as crustaceans and insects, crabs, cephalopods, and scales of fish, and Lissamphibia [11]. Filling Chitosan matrix with Ag nanoparticles has immense potential in medicine, especially in wound dressings, because of its antimicrobial properties. Where the chitosan matrix would help control the release of Ag nanoparticles, thereby reducing the Ag toxicity to normal cells [12].

PVA, PVP, and chitosan are used as capping agents to regulate the nanoparticle shape and size and to impart stability for the synthesized Ag nanomaterials. Also, PVA and PVP are used as reducing agents which provide free electrons to reduce Ag ions and form Ag nanoparticles [13].

The aim of the present study is to synthesize novel composite membrane from a PVP/PVA/chitosan blend filled with different concentrations of silver nanoparticles (green synthesized and laser-ablated), with a simple method for the production and investigation of their physical properties. An in-depth study of the optical and structural properties of this system is discussed using various techniques and tools.

2. Experimental Work

2.1. Materials

PVA (provided by S.D. Fine-Chem India – 14000 MW), PVP (provided by SISCO Research Laboratory India – 40000 MW), and chitosan (from Fluka, USA) were utilised as blend matrix for filling with AgNPs (synthesized by green chemistry and femtosecond laser ablation method); the distilled water was used as solvent.

2.2. Samples preparation

Silver nanoparticles were prepared as previously described in previous work [14–17]. Separately, PVA and PVP were dissolved in distilled water and agitated at 65°C for about 5h, while chitosan was prepared by dissolving in distilled water containing 2% acetic acid. They are mixed to form a blend from 40% by weight of PVA, 40% by weight of PVP, and 20% by weight of chitosan.

The AgNPs in distilled water were combined with the polymer blend in precalculated amounts under the same conditions to obtain samples of nanocomposite with different concentrations of AgNP as shown in Table 1. After that, the solution was placed into Petri plates at 45°C for approximately 48h. After complete drying, the nanocomposite films were peeled off from the Petri dishes and preserved in desiccators under vacuum until their use.

Table (1): sample nomination and composition

	PVP	PVA	Chitosan	Blend	L-green AgNPs (1%)	H-green AgNPs (5%)	L-ablated AgNPs (1%)	L-ablated AgNPs (5%)
					ml · 280 ppm/w			
PVP	100	0.0	0.0	40	39.6	38	39.6	38
PVA	0.0	100	0.0	40	39.6	38	39.6	38
Chitosan	0.0	0.0	100	20	19.8	19	19.8	19
AgNP's	0.0	0.0	0.0	0.0	1	5	1	5

2.3. Physical characterization

PANalytical X'Pert PRO XRD was used to record X-ray diffraction (XRD) scans of the prepared samples using a Cu-K target with a wavelength of 1.54 Å and a voltage of 45 kV. The Fourier-transform infrared spectroscopy (FTIR) data were collected within the spectral region 4000 – 400 cm^{-1} at room temperature using Nicolet iS10 FTIR single-beam spectrometer. Electronic spectra in the wavelength range of 200 to 1100 nm were measured via (JASO V570) double beam spectrophotometer using air as the reference. A transmission electron microscope was used to scan the size and shape of the nanoparticles (JEOL-JEM-1011, Japan).

3. Results And Discussion

3.1. Fourier transform infrared (FTIR)

FTIR spectra of chitosan, PVP, PVA, unfilled and filled PVP/PVA/chitosan blends with different AgNP contents were shown in Figure (1). The spectra revealed the characteristic peaks of bending and stretching vibrations for the functional groups found in the prepared films. Table 2 shows the peak positions of the FTIR absorption bands and their assignments for the produced films.

In the case of pure PVA, the broadness and absorbance at about 3265 cm^{-1} are attributed to the stretching vibration of the hydroxyl groups (OH) of PVA [18, 19]. The asymmetric CH_2 stretching vibration is responsible for the peak at 2938 cm^{-1}. The bands at 1710 and 1661 cm^{-1} were assigned to the C = O and C = C stretching modes [19, 20]. The absorption peak at 1420 cm^{-1} was attributed to the CH_2 symmetrical bending, while the peak at 1327 cm^{-1} is assigned to (CH + OH) bending [21]. The C–O stretch of the carbonyl groups in the PVA backbone corresponds to the band at about 1088 cm^{-1}. The peak at 842 cm^{-1} has been assigned to C-C stretching vibrations with moderate absorption. The OH wagging is responsible for the peak at 593 cm^{-1}, whereas the CH_2 rocking is responsible for the peak at 917 cm^{-1} [20].

For PVP, the absorbance observed at 3396 cm^{-1} are attributed to (OH) stretching [22], while the absorbance at 1437 cm^{-1} and 843 cm^{-1} correspond respectively to the CH_2 scissoring vibrations and CH_2 bending. C = O stretching and C–N stretching are given to the peaks at 1644 cm^{-1} and 1017 cm^{-1}, respectively [23–25].

Chitosan spectra showed a peak at 3290 cm^{-1} is attributed to OH stretching, while at 2875 cm^{-1} is attributed to CH_2 stretching. The vibrational mode of amide C□O stretching was observed at 1654 cm^{-1} [26]. C–O–C stretching is assigned to the peak at 1151 cm^{-1}, while NH out-of-plane bending is assigned to the peak at 561 cm^{-1} [27].

In the PVP/PVA/chitosan blend sample, most intensities of the absorption peaks differed irregularly from their values in the individual polymers. Furthermore, the hydroxyl groups of the blend showed a decrease in intensity and a shift to a lower wavenumber 3280 cm^{-1} because of the hydrogen linking formation between the OH group (of PVA and chitosan) with the C = O of PVP, ensuring the miscibility of the prepared blend [28, 29]. In the spectra of the PVP/PVA/chitosan blend filled with AgNPs we could not observe any specific bands for AgNPs in the range between 4000 – 400 cm^{-1}. Since their absorption occurs in far-infrared only that is in the range (400 – 100 cm^{-1}) [30]. We, therefore, discuss the AgNPs incorporation in the PVP/PVA/chitosan blend and the interaction between the bonds of the blend and AgNPs.

It may be visualized that in figure (1_b&c) there is new small broadband at 3746 cm^{-1} and a small sharp peak at 414 cm^{-1} with increasing in AgNPs content. For the highest content of AgNPs filling (H green and H laser-ablated), the peak at 2859 cm^{-1} reappeared which is one of the characteristic peaks of chitosan (CH2 symmetric stretching). There is also a marked change in intensity with a small shift in most peaks in the major characteristic bands of the PVP/PVA/chitosan blend compared to that filled with various contents of AgNPs, which mean that the AgNPs have highly interacted with hydrogen bonds in PVP/PVA/chitosan spectra.

Table (2): FTIR absorption bands and their assignments for a) pure PVA, b) pure PVP, c) Chitosan and d) unfilled and filled PVP/PVA/chitosan blend with AgNPs.

Band assignment	Wavenumber (cm^{-1})				Ref.
	PVA	PVP	Chitosan	Blend	
OH stretching	3265	3396	3290	3280	[18, 19, 22, 31, 32]
N–H stretching of secondary amide			2974		[32]
CH2 asymmetric stretching	2938	2949		2933	[19, 20, 23, 31]
CH2 symmetric stretching	2908	2859	2875		[19, 20, 22, 27, 33]
C = O stretching	1710	1644	1645	1644	[19, 20, 22, 24, 33]
C = C stretching	1661				[19, 20]
N-H bending (amide II band)			1563		[32, 33]
characteristic vibration of C = N (pyridine ring)		1493			[23, 31]
CH2 bending	1420	1461, 1422, 1372, 843	1416	1422	[20, 23, 24, 27, 31, 33–35]
CH2 scissoring vibrations		1437			[23, 31]
CH wagging	1374, 1238	1287		1287	[19, 20, 23, 31]
(CH + OH) bending	1327				[20]
C-C stretching	1140, 842	1217, 933		842	[19, 20, 24, 36]
Asymmetric bridge oxygen stretching (glycosidic linkage)			1151		[33]
C-O stretching	1088			1088	[20]
C–O bending	476		1044		[20, 27, 33]
C–N stretching vibrations		1017	881		[25, 27]
CH2 rocking	917	733			[20, 24]
OH wagging	593				[20]
N-H bending			561		[27]
CO wagging	417				[20]

Band assignment	Wavenumber (cm^{-1})				Ref.
	PVA	PVP	Chitosan	Blend	
C–N bending		645			[31]
N-C = O bending			568	568	[37]

3.2. X-ray diffraction (XRD)

Figure (2a) explains the XRD for pure chitosan, PVP, PVA, and the blend, while Figure (2b) reveals the XRD of blend films filled with different concentrations of AgNPs in the extented 2θ range between 3° and 70°. The XRD of the pure PVA reveals diffraction peaks at 2θ = 19.4° and 40.4° due to the partially crystalline nature of the PVA structure supported by intermolecular and intramolecular hydrogen bonds. PVA exhibits as well a low intensity diffraction peak at 2θ = 22.7^{o} [38]. The chitosan film has a broad diffraction peak at 2θ = 23^{o}, while PVP has very broad diffraction peaks at 2θ = 11° and 22°, confirming the amorphous nature of the chitosan and PVP films examined [39].

For the unfilled PVP/PVA/chitosan blend, it can be seen that the intensity of the peak at 2θ = 19.4° has reduced and become broader. This means that adding PVP and chitosan to PVA reduces the semi-crystalline nature of PVA and indicates high compatibility between the components of the blend.

Filling the blend with AgNPs also reduces the peak intensity at 2θ = 19.4°, which is based on the interaction between the filler and the blend, resulting in less intermolecular interaction between the blend chains and a decrease in the degree of crystallization [22]. This amorphous nature is responsible for the higher ionic diffusion resulting in higher ionic conductivity [40]. This behavior indicates that the PVA/PVP/chitosan blend matrix has been structurally modified as a result of the AgNPs filling and confirms the results obtained in the FTIR studies (section 3.1).

Moreover, it can be seen from the same figure that after filling with a high content of ablated AgNPs, a new peak is generated at ~ 38^{o}, which can be attributed to the Face centred cubic (fcc) structure of the embedded AgNPs, which corresponds to h k l parameters (111) [41].

3.3. Transmission electron microscopy (TEM)

To ensure the size and morphology of the produced AgNPs, transmission electron microscopy (TEM) was used. Figures (3) displays the transmission electron microscopic images for the purely green and laser-ablated AgNPs in aqueous solution, revealing that the nanoparticles are roughly rectangular, randomly distributed, and have diameters ranging from 30 to 100 nm.

3.4. UV/Vis. absorption and optical studies

Figure (4) displays the UV/visible absorption spectra of the pristine, blend, and nanocomposite film samples.

The spectra of pure chitosan show an absorption band at 208 nm, which can be assigned to the chromatic functional groups (NHCOR) and/or the presence of chromophore groups (C = C) or (C = O) [42], while pure PVA shows an absorbance peak at ~ 200 nm, that is attributed to an n → π* transition. The PVA transition is associated with the carbonyl groups (C = O) related to ethylene unsaturation (C = C) of the (CH = CH)CO– type. The presence of carbonyl functionalities might be because of residual acetate groups remaining after the PVA fabrication with the aid of using hydrolysis of polyvinyl acetate or oxidation throughout fabrication and processing [43].

After adding AgNPs (Fig. 5), the nanocomposite samples give a significant increase in the absorbance values at 200 nm with a gradual red shift to longer wavelengths as the AgNPs content increase. This can be assigned to the interaction between polymeric matrices and the added AgNPs affecting the calculated optical bandgap [44] associated with the crystallinity change in the nanocomposite, as discussed earlier in Section 3.2. In addition, a peak begins to appear at λ_{max} = 427 nm, and its intensity continuously increases with the increase of AgNPs concentration. The appearance of this peak in the visible range is caused by the surface plasmon resonance (SPR) nature of the AgNPs inserted in a dielectric medium, which results from the collective excitation of the conduction band electrons in the nanoparticle. The presence of these beaks also indicates that the fabricated blend can be used as a good cabbing agent for the AgNPs. The increase in λ_{max} (and hence decrease in its optical bandgap energy) mean that the particle size increases as the filler concentration increase [45], indicating that the laser-ablated Ag nanoparticles have a greater size than the obtained from green prepared Ag nanoparticles.

The optical energy gap (E_g) can be estimated using the Mott and Davis equation [46], which analyzes the spectral dependence of the absorption coefficient near the absorption edge.

$$\alpha = \frac{A(h\upsilon - E_g)^r}{h\upsilon} (1)$$

where A is a constant associated with the electronic transition probability, $h\upsilon$ is the energy of the incident photons, and the power r is related to the transition behavior and equal to 2 or ½ for the allowed direct and indirect transition, respectively.

Figures 6a and 6b show a plot of $(\alpha h\upsilon)^2$ and $(\alpha h\upsilon)^{1/2}$ with hυ for the prepared samples. Extrapolating the linear fit lines in these data points on the hυ axis yields the optical band gap values, which are listed in table 3.

It is evident that the calculated optical bandgaps decrease with increasing AgNPs content and are assigned to the role of AgNPs in modulating the structure caused by the formation of variable polaronic

and defect levels that are related to localized states density $\mathrm{N(E)}$ [47].

At lower energies below the fundamental absorption edge, spectral data revealed the appearance of an elongated tail that correlates with the localized states in the valence band tail, attributed to defects formed by AgNPs, and extends to states in the conduction band. In such a case, the absorption coefficient α can be entirely attributed to the energy tail width $\Delta \mathrm{E}$ and the photon energy which is thermal vibration in the lattice [20] and can be determined by Urbach formula [48].

$$\alpha = \alpha_o exp\left(\frac{\mathrm{h}\upsilon}{\Delta E}\right) (2)$$

where $\alpha_{\mathrm{o}}$is a constant

Urbach energy $(\Delta \mathrm{E})$ values can be obtained by plotting the logarithm of the absorption coefficient against photon energy $(\mathrm{h}\upsilon)$ as shown in Figure (7) and listed in Table 3. For the pure blend, the value of $\Delta \mathrm{E}$is 0.16 eV and that of the filled samples is increased up to 0.23 eV.

The increase in Urbach energy confirms the increase in the width of localized states within the bandgap and hence, is responsible for bandgap decay of the filled samples.

Table (3): indirect optical energy gab Egid direct optical energy gab E_{gd}, and Urbach Energy $\Delta \mathrm{E}$ of the prepared blend filled with AgNPs

Sample	$\mathrm{E_{gid}(eV)}$	$\mathrm{E_{gd}(eV)}$	$\mathrm{\Delta E(eV)}$
Blend	4.94	5.25	0.16
L Ag green	4.93	5.24	0.16
L Ag ablated	4.91	5.21	0.17
H Ag green	4.87	5.20	0.18
H Ag ablated	4.85	5.19	0.23

3.5. Antibacterial studies

Antibacterial characteristics of the studied samples containing both high and low-level dopant of both green synthesized and silver ablated nanoparticles were performed against two gram-positive and two gram-negative bacteria namely E. Coli, Pseudomonas aeuroginosa, S. aureus, and B. Cereus. The minimum inhibition zone (MIZ) agar diffusion method was used. Polymeric samples with nearly equal diameter were seeded in the bacterial medium and incubated at 37°C for 24h. Sample concentrations and their corresponding inhibition zone in (mm) were listed in the table (4).

Table (4) Sample concentrations and their corresponding inhibition zone in (mm)

Sample	*E. coli*	*Pseudomonas aeuroginosa*	*S. aureus*	*B. cereus*
Blend	12	12	11	11
Green L	13	14	13	12
Green H	14	15	15	14
Laser L	15	17	17	16
Laser H	15	17	18	17

Obtained data shows the effect of adding silver nanoparticles to the polymeric matrix. It was noticed that the inhibition zone in the case of samples containing silver nanoparticles is generally increasing and the result appears promising and with higher value, in the case of ablated laser, this may be attributed to both the size and monodisperse distribution of the nanoparticle. It was also clear that the effect of all samples against gram-positive bacteria is slightly increasing than that of gram-negative bacteria as shown in Fig. 8. Such behavior can be considered in terms of the rapid generation of free radicals through redox reaction while ROS can react directly with membrane components including proteins, lipids, and DNA that are scavenged by antioxidants resulting in oxidative stress in bacterial cells [49].

4. Conclusion

The PVP/PVA /chitosan blend filled with different contents of silver nanoparticles was made by a common casting technique. X-ray analysis showed that after filling with highly ablated AgNPs, a peak at 38^{o} is generated, which can be attributed to the face-centered-cubic structure (fcc) of the embedded silver nanoparticles, which corresponds to h k l parameters (111). UV/visible and FTIR spectroscopic data revealed the interaction and complexation with the prepared polymers and /or AgNPs, which can be seen in the growth and red shift of the UV band, which can be attributed to the intermolecular interaction between hydrogen bonds. It has been shown that the optical band gaps are considerably reduced by the filling, where the filling with silver nanoparticles forms the levels of traps rich in charge carriers. All of these data support the idea of complexation between AgNPs and the blend matrix. TEM images

confirmed the exsitence of silver nanoparticles with a diameter between 30 and 100 nm. The blend and the Ag-nanocomposite showed good antibacterial activity and caused a significant decrease in microbial growth (Escherichia coli) in 24 hours.

References

1. D. Garibo, H.A. Borbón-Nuñez, J.N.D. de León, E. García Mendoza, I. Estrada, Y. Toledano-Magaña, H. Tiznado, M. Ovalle-Marroquin, A.G. Soto-Ramos, A. Blanco, J.A. Rodríguez, O.A. Romo, L.A. Chávez-Almazán, A. Susarrey-Arce, Green synthesis of silver nanoparticles using Lysiloma acapulcensis exhibit high-antimicrobial activity. Sci. Rep. **10**, 12805 (2020)
2. S.-H. Min, G.-Y. Lee, S.-H. Ahn, Direct printing of highly sensitive, stretchable, and durable strain sensor based on silver nanoparticles/multi-walled carbon nanotubes composites. Compos. Part B: Eng. **161**, 395–401 (2019)
3. S. Sreeja, S. Prabhakaran, B. Pesala, Efficiency Enhancement of Betanin Dye-Sensitized Solar Cells Using Plasmon-Enhanced Silver Nanoparticles, in *Advances in Energy Research*, vol. 1, ed. by S. Singh, V. Ramadesigan (Springer Singapore, Singapore, 2020), pp. 9–18
4. L. Mo, Z. Guo, L. Yang, Q. Zhang, Y. Fang, Z. Xin, Z. Chen, K. Hu, L. Han, L. Li, Silver nanoparticles based ink with moderate sintering in flexible and printed electronics. Int. J. Mol. Sci. **20**, 2124 (2019)
5. A.L. Waly, A.M. Abdelghany, A.E. Tarabiah, Study the structure of selenium modified polyethylene oxide/polyvinyl alcohol (PEO/PVA) polymer blend. J. Mater. Res. Technol. **14**, 2962–2969 (2021)
6. M.I. Baker, S.P. Walsh, Z. Schwartz, B.D. Boyan, A review of polyvinyl alcohol and its uses in cartilage and orthopedic applications. J. Biomedical Mater. Res. Part B: Appl. Biomaterials **100**, 1451–1457 (2012)
7. E.M. Abdelrazek, A.M. Abdelghany, A.E. Tarabiah, H.M. Zidan, AC conductivity and dielectric characteristics of PVA/PVP nanocomposite filled with MWCNTs. J. Mater. Sci.: Mater. Electron. **30**, 15521–15533 (2019)
8. M. Kurakula, G.S.N.K. Rao, Pharmaceutical assessment of polyvinylpyrrolidone (PVP): As excipient from conventional to controlled delivery systems with a spotlight on COVID-19 inhibition. J. Drug Deliv. Sci. Technol. **60**, 102046 (2020)
9. M. Voronova, N. Rubleva, N. Kochkina, A. Afineevskii, A. Zakharov, O. Surov, Preparation and Characterization of Polyvinylpyrrolidone/Cellulose Nanocrystals Composites, Nanomaterials 8 (2018)
10. F. Gami, N. Algethami, H.M. Ragab, A. rajah, A.E. Tarabiah, Structural, optical and electrical studies of chitosan/polyacrylamide blend filled with synthesized selenium nanoparticles. J. Mol. Struct. **1257**, 132631 (2022)
11. N. Morin-Crini, E. Lichtfouse, G. Torri, G. Crini, Applications of chitosan in food, pharmaceuticals, medicine, cosmetics, agriculture, textiles, pulp and paper, biotechnology, and environmental chemistry. Environ. Chem. Lett. **17**, 1667–1692 (2019)

12. A. Mohandas, S. Deepthi, R. Biswas, R. Jayakumar, Chitosan based metallic nanocomposite scaffolds as antimicrobial wound dressings. Bioactive Mater. **3**, 267–277 (2018)
13. K. Varner, J. Sanford, A. El-Badawy, D. Feldhake, R. Venkatapathy, State of the science literature review: everything nanosilver and more, US Environmental Protection Agency, Washington DC 363 (2010)
14. A.M. Abdelghany, A.A. Menazea, M.A. Abd-El-Maksoud, T.K. Khatab, Pulsed laser ablated zeolite nanoparticles: A novel nano-catalyst for the synthesis of 1, 8-dioxo-octahydroxanthene and N-aryl-1, 8-dioxodecahydroacridine with molecular docking validation. Appl. Organomet. Chem. **34**, e5250 (2020)
15. A.A. Al-Shamari, A.M. Abdelghany, H. Alnattar, A.H. Oraby, Structural and optical properties of PEO/CMC polymer blend modified with gold nanoparticles synthesized by laser ablation in water. J. Mater. Res. Technol. **12**, 1597–1605 (2021)
16. F.R. El Awady, M.A. Abbas, A.M. Abdelghany, Y.A. El-Amier, Silver Modified Hydrophytes for Heavy Metal Removal from Different Water Resources. Biointerface Res. Appl. Chem. **11**, 14555–14563 (2021)
17. A.M. Abdelghany, A.H. Oraby, M.O. Farea, Influence of green synthesized gold nanoparticles on the structural, optical, electrical and dielectric properties of (PVP/SA) blend. Phys. B: Condens. Matter **560**, 162–173 (2019)
18. S. Luo, X. Qiao, Q. Wang, Y. Zhang, P. Fu, Z. Lin, F. Du, C. Cheng, Excellent self-healing and antifogging coatings based on polyvinyl alcohol/hydrolyzed poly(styrene-co-maleic anhydride). J. Mater. Sci. **54**, 5961–5970 (2019)
19. G.M. Kim, A.S. Asran, G.H. Michler, P. Simon, J.S. Kim, Electrospun PVA/HAp nanocomposite nanofibers: biomimetics of mineralized hard tissues at a lower level of complexity. Bioinspir. Biomim. **3**, 046003 (2008)
20. I. Omkaram, R.P.S. Chakradhar, J.L. Rao, EPR, optical, infrared and Raman studies of VO2 + ions in polyvinylalcohol films. Phys. B: Condens. Matter **388**, 318–325 (2007)
21. A.M. Abdelghany, E.M. Abdelrazek, A.E. Tarabiah, Modeling and physical properties of lead sulphide/polyvinyl alcohol nano-composite. Quantum Matter **5**, 257–262 (2016)
22. E.M. Abdelrazek, I.S. Elashmawi, S. Labeeb, Physica B 405 (2010) 2021
23. A.M. Abdelghany, E.M. Abdelrazek, S.I. Badr, M.A. Morsi, Mater. Des. **97**, 532 (2016)
24. I.S. Elashmawi, E.M. Abdelrazek, A.Y. Yassin, Br. J. Appl. Sci. Technol. **4**, 4263 (2014)
25. M. Kumar, P. Devi, A. Kumar, Structural analysis of PVP capped silver nanoparticles synthesized at room temperature for optical, electrical and gas sensing properties. J. Mater. Sci.: Mater. Electron. **28**, 5014–5020 (2017)
26. N. Algethami, A. Rajeh, H.M. Ragab, A.E. Tarabiah, F. Gami, Characterization, optical, and electrical properties of chitosan/polyacrylamide blend doped silver nanoparticles, Journal of Materials Science: Materials in Electronics (2022)

27. R. Varma, S. Vasudevan, Extraction, Characterization, and Antimicrobial Activity of Chitosan from Horse Mussel Modiolus modiolus. ACS Omega **5**, 20224–20230 (2020)
28. D. Mondal, M.M.R. Mollick, B. Bhowmick, D. Maity, M.K. Bain, D. Rana, A. Mukhopadhyay, K. Dana, D. Chattopadhyay, Effect of poly (vinyl pyrrolidone) on the morphology and physical properties of poly (vinyl alcohol)/sodium montmorillonite nanocomposite films. Progress in Natural Science: Materials International **23**, 579–587 (2013)
29. E. Karavas, E. Georgarakis, D. Bikiaris, Adjustingdrug release by using miscible polymer blends as effective drug carries. J. Therm. Anal. Calorim. **84**, 125–133 (2006)
30. A. Fielicke, I. Rabin, G. Meijer, Far-Infrared Spectroscopy of Small Neutral Silver Clusters. J. Phys. Chem. A **110**, 8060–8063 (2006)
31. E.M. Abdelrazek, A.M. Abdelghany, S.I. Badr, M.A. Morsi, Structural, optical, morphological and thermal properties of PEO/PVP blend containing different concentrations of biosynthesized Au nanoparticles. J. Mater. Res. Technol. **7**, 419–431 (2018)
32. E.M. Abdelrazek, I.S. Elashmawi, S. Labeeb, Chitosan filler effects on the experimental characterization, spectroscopic investigation and thermal studies of PVA/PVP blend films. Phys. B: Condens. Matter **405**, 2021–2027 (2010)
33. T.K. Varun, S. Senani, N. Jayapal, J. Chikkerur, S. Roy, V.B. Tekulapally, M. Gautam, N. Kumar, Extraction of chitosan and its oligomers from shrimp shell waste, their characterization and antimicrobial effect. Veterinary world **10**, 170 (2017)
34. V. Sharma, D. Verma, G.S. Okram, Influence of surfactant, particle size and dispersion medium on surface plasmon resonance of silver nanoparticles. J. Phys.: Condens. Matter **32**, 145302 (2020)
35. V.K. Singh, B. Bhattacharya, S. Shukla, P.K. Singh, Mater. Technol. **49**, 123 (2015)
36. M. Ravi, Y. Pavani, K. Kiran Kumar, S. Bhavani, A.K. Sharma, V.V.R. Narasimha Rao, Studies on electrical and dielectric properties of PVP:KBrO4 complexed polymer electrolyte films. Mater. Chem. Phys. **130**, 442–448 (2011)
37. D. Kamaruddin, I. Edikresnha, M.M. Sriyanti, Munir, Khairurrijal, Synthesis of Polyvinylpyrrolidone (PVP)-Green Tea Extract Composite Nanostructures using Electrohydrodynamic Spraying Technique, IOP Conference Series: Materials Science and Engineering 202 (2017) 012043
38. A.A. Menazea, A.M. Ismail, N.S. Awwad, H.A. Ibrahium, Physical characterization and antibacterial activity of PVA/Chitosan matrix doped by selenium nanoparticles prepared via one-pot laser ablation route. J. Mater. Res. Technol. **9**, 9598–9606 (2020)
39. K. Sivaiah, K.N. Kumar, V. Naresh, S. Buddhudu, Mater. Sci. Appl. **2**, 1688 (2011)
40. H. Zidan, N. El-Ghamaz, A. Abdelghany, A. Lotfy, Structural and Electrical Properties of PVA/PVP Blend Doped with Methylene Blue Dye. Int. J. Electrochem. Sci. **11**, 9041–9056 (2016)
41. K. Jyoti, M. Baunthiyal, A. Singh, Characterization of silver nanoparticles synthesized using Urtica dioica Linn. leaves and their synergistic effects with antibiotics. J. Radiation Res. Appl. Sci. **9**, 217–227 (2016)

42. A.M. Abdelghany, A.A. Menazea, A.M. Ismail, Synthesis, characterization and antimicrobial activity of Chitosan/Polyvinyl Alcohol blend doped with Hibiscus Sabdariffa L. extract. J. Mol. Struct. **1197**, 603–609 (2019)
43. H.H. Saleh, D.E. El-Hadedy, G.A. Meligi, T.A. Afify, J. Sci. Res. **5**, 151 (2013)
44. D. Fink, *Fundamentals of Ion-Irradiated Polymers* (Springer-Verlag, Heidelberg (Berlin), 2004)
45. E. Saion, E. Gharibshahi, K. Naghavi, Int. J. Mol. Sci. **14**, 7880 (2013)
46. J. Tauc, *Amorphous and liquid semiconductors* (Plenum Press, New York, 1974)
47. R. Murri, L. Schiavulli, N. Pinto, T. Ligonzo, Urbach tail in amorphous gallium arsenide films. J. Non-cryst. Solids **139**, 60–66 (1992)
48. F. Urbach, The Long-Wavelength Edge of Photographic Sensitivity and of the Electronic Absorption of Solids. Phys. Rev. **92**, 1324–1324 (1953)
49. M.A. Quinteros, V.C. Aristizábal, P.R. Dalmasso, M.G. Paraje, P.L. Páez, Oxidative stress generation of silver nanoparticles in three bacterial genera and its relationship with the antimicrobial activity. Toxicol. In Vitro **36**, 216–223 (2016)

Figures

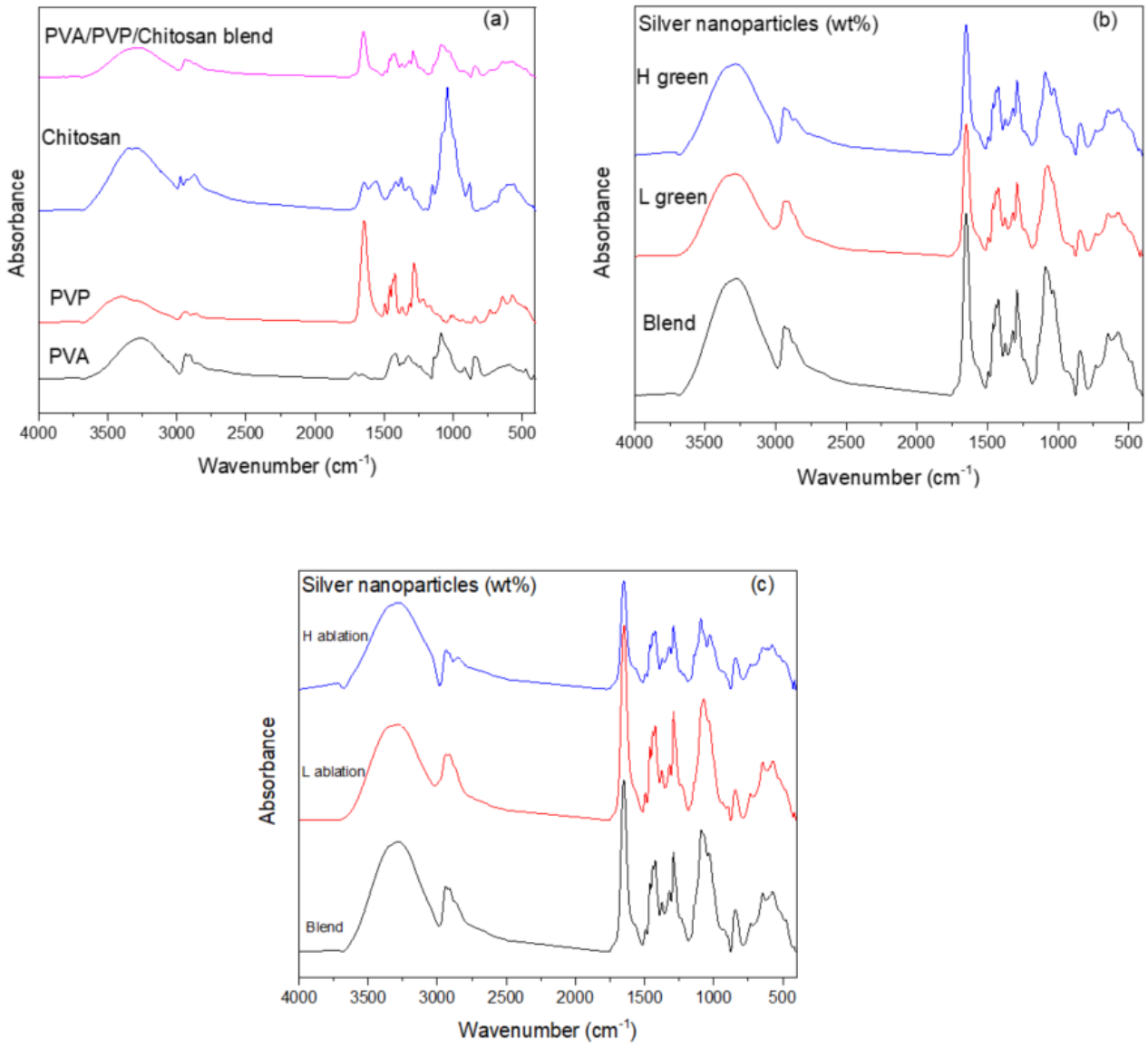

Figure 1

FTIR absorbance spectra of a) pure PVA, pure PVP, pure chitosan, unfilled PVP/PVA/chitosan blend, b) unfilled and filled PVP/PVA/chitosan blend with silver nanoparticles green Synthesized c) unfilled and filled PVP/PVA/chitosan blend with silver nanoparticles Laser Ablated.

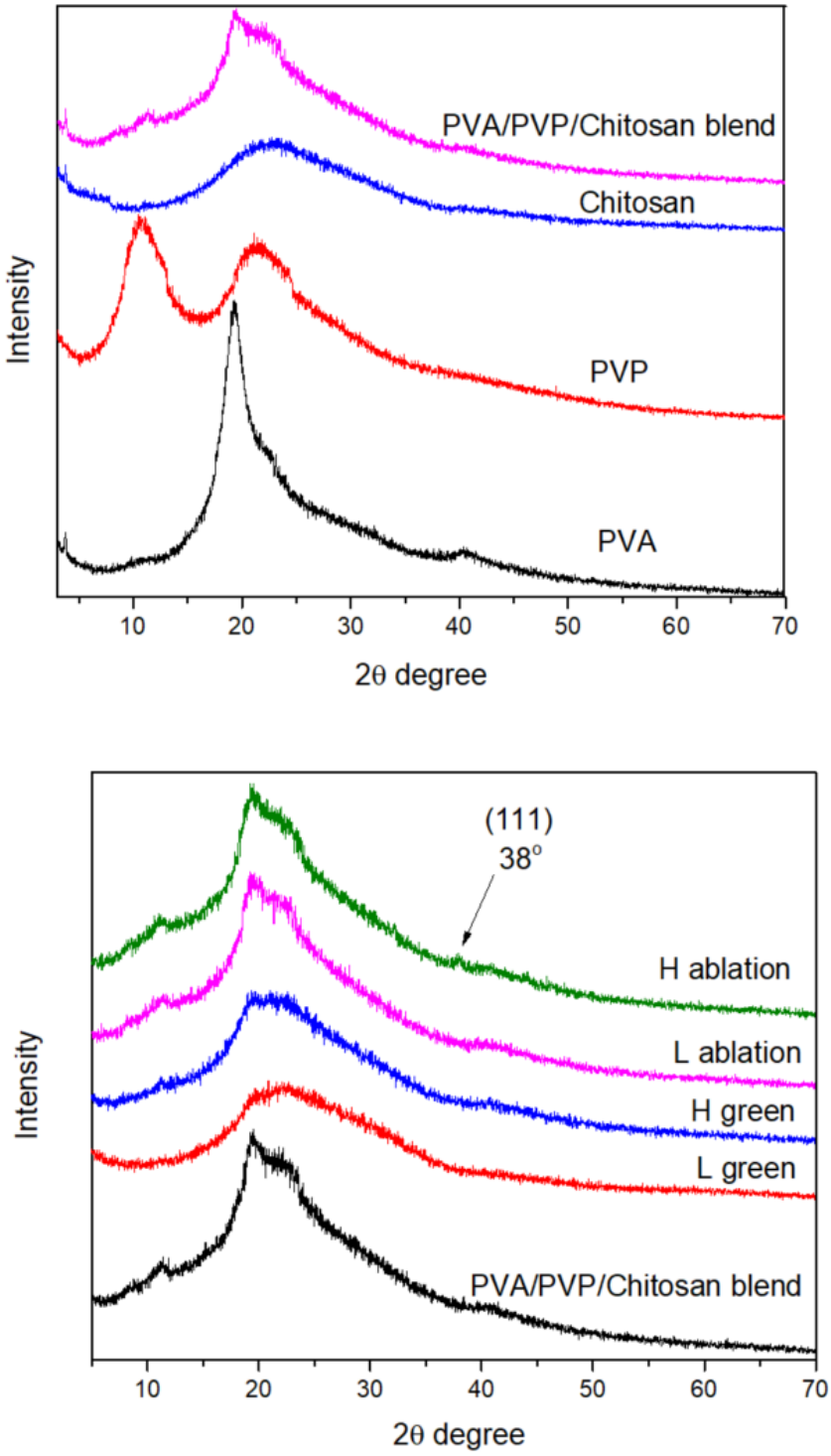

Figure 2

X-ray diffraction pattern for a) pure PVA, pure PVP, pure chitosan, unfilled PVP/PVA/chitosan blend, and b) unfilled and filled PVP/PVA/chitosan blend with silver nanoparticles.

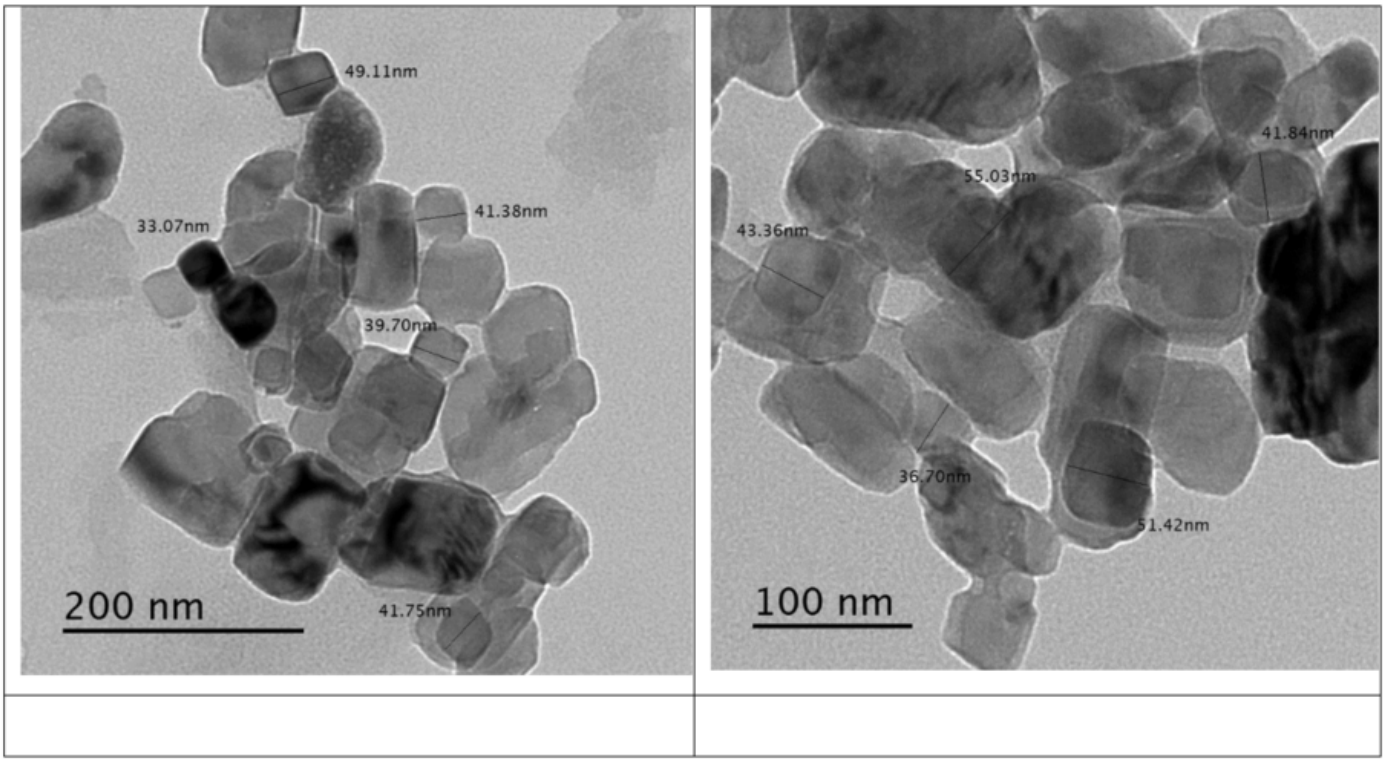

Figure 3

TEM images for green and laser-ablated AgNPs.

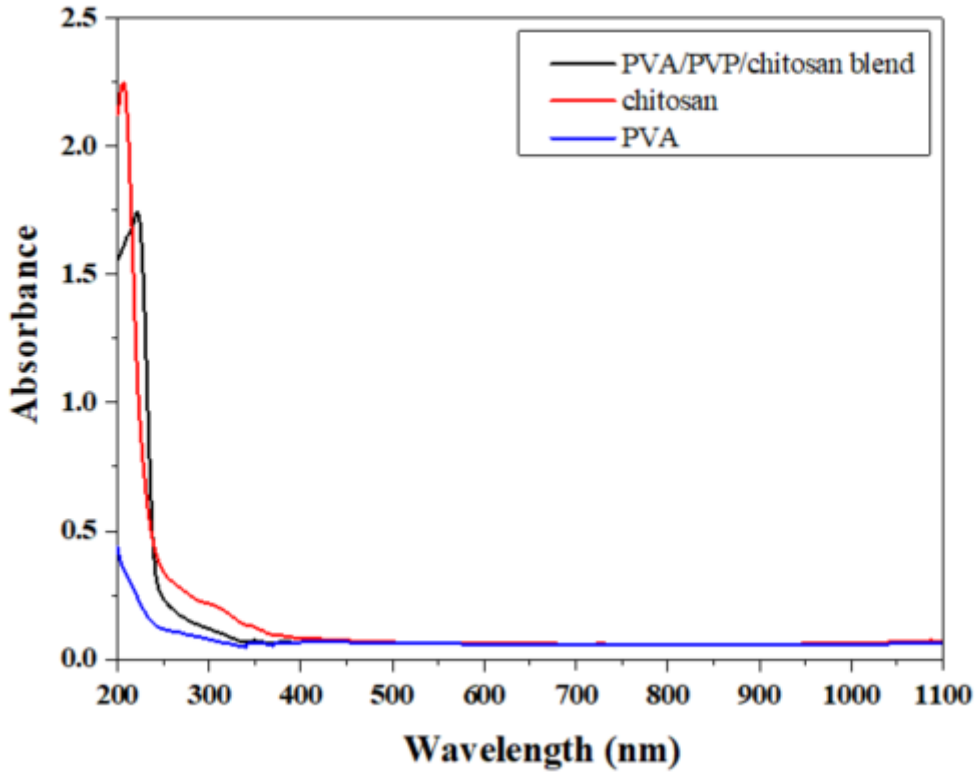

Figure 4

UV/visible absorbance spectra for pure PVA, pure chitosan and pure PVP/PVA/ chitosan blend.

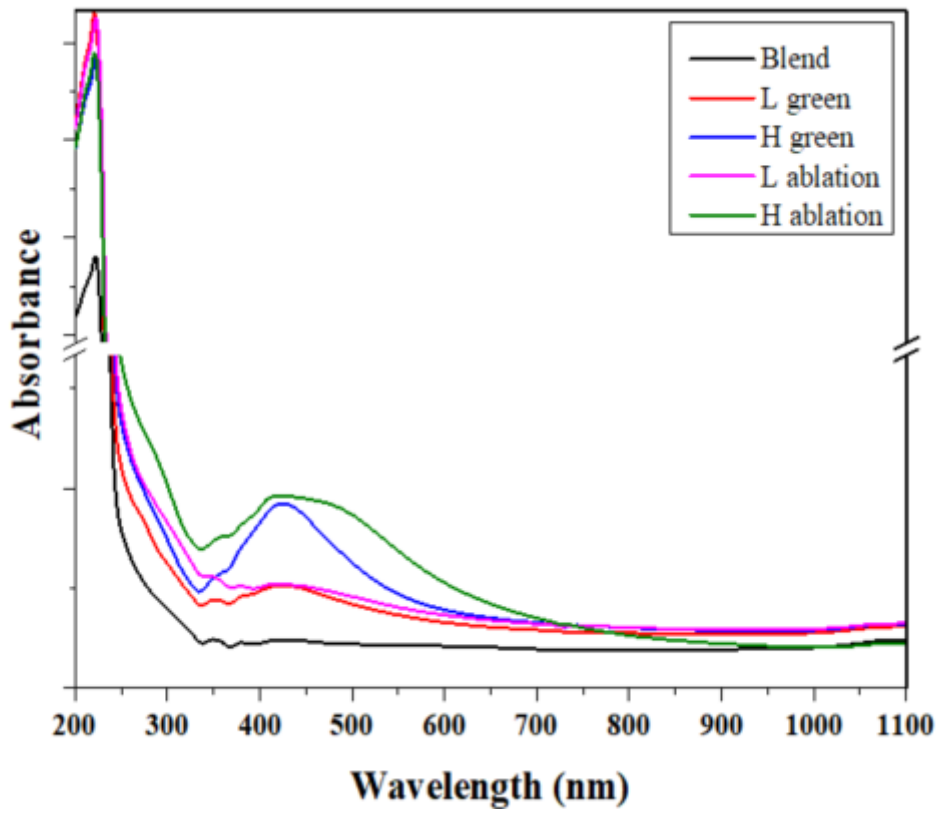

Figure 5

UV/visible absorbance spectra for unfilled and filled PVP/PVA/chitosan blend with Ag nanoparticles.

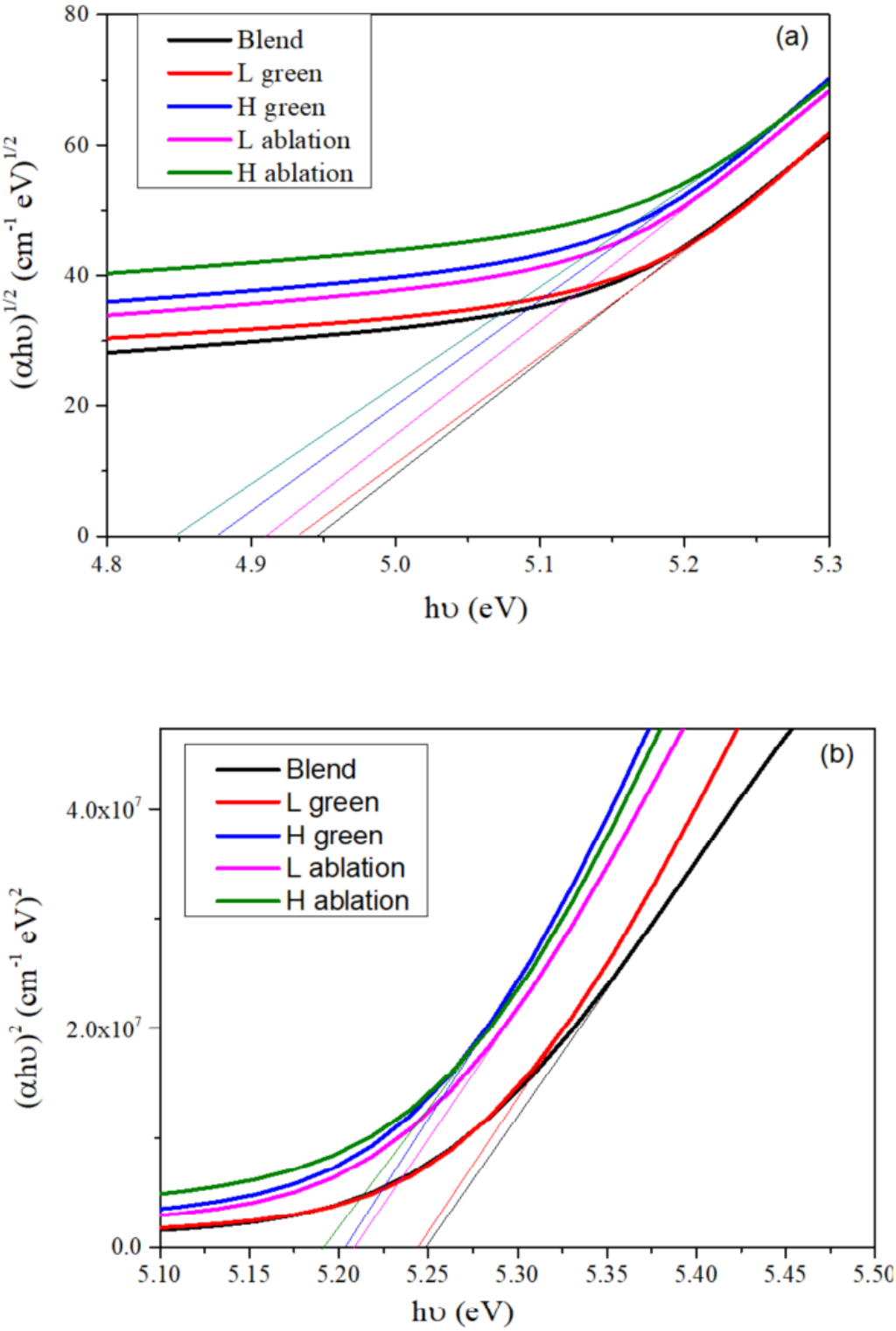

Figure 6

The plots of a) and b) versus for the blend filled with different contents of AgNPs.

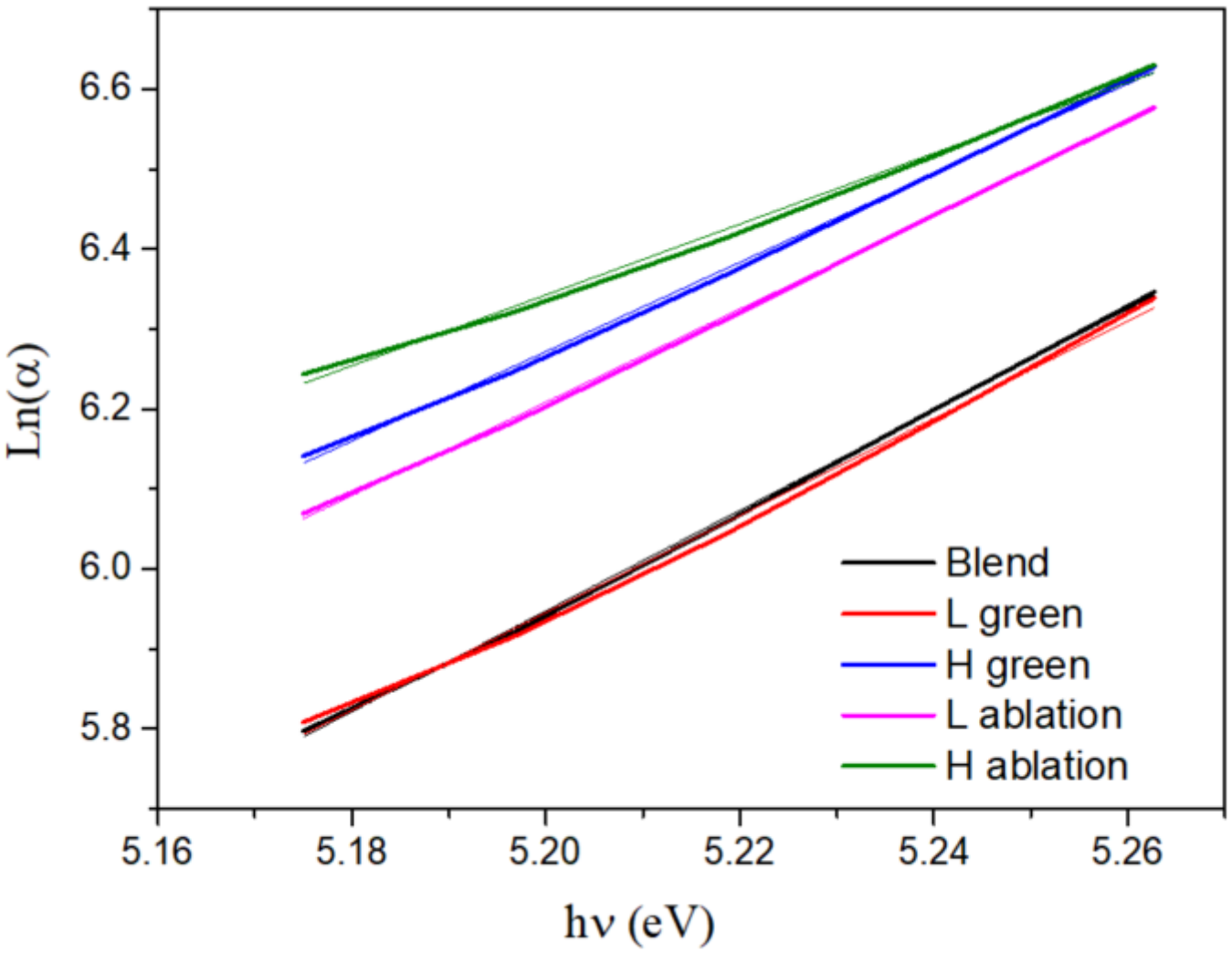

Figure 7

Logarithm of absorption coefficient versus photon energy for the blend filled with different contents of AgNPs.

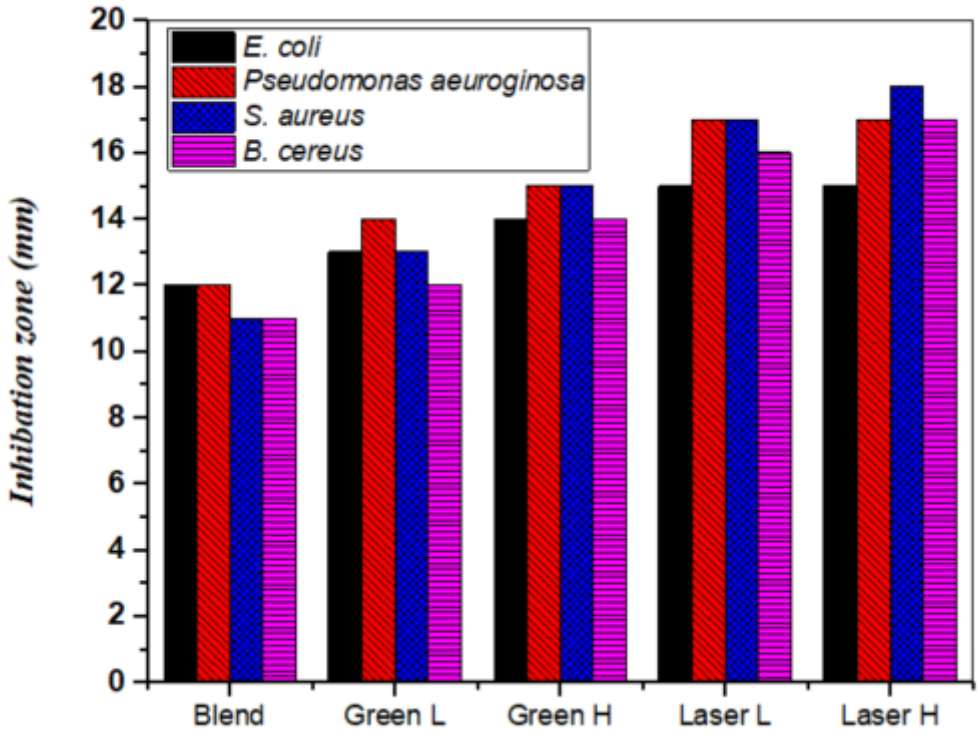

Figure 8

correlation between sample concentrations and their corresponding inhibition zone in (mm)